RSC Sustainability

ROYAL SOCIETY OF CHEMISTRY

PAPER

View Article Online
View Journal | View Issue

Cite this: *RSC Sustainability*, 2024, **2**, 459

Self-assembled lignin nanoparticles produced from elephant grass leaves enable selective inactivation of Gram-positive microorganisms†

Isabella C. Tanganini,[ab] Camilla H. M. Camargos,[cd] Jennifer C. Jackson,[a] Camila A. Rezende,[c] Sandra R. Ceccato-Antonini[e] and Andreia F. Faria *[a]

In this study, we added value to lignocellulosic biomass-derived lignin by converting it into antimicrobial nanoparticles using a simple self-assembling method in solution. Transmission electron microscopy (TEM) and zeta potential analyses showed that the self-assembled lignin nanoparticles (SA-LNPs) had a spherical-like morphology, 80 nm average size, and a surface charge of −29 ± 4 mV. Previous studies have shown that LNPs are toxic to bacteria, though the potential mechanisms of action leading to antimicrobial properties of LNPs are lacking in the literature. Therefore, we conducted a thorough investigation of the antibacterial activity of SA-LNPs using four bacteria strains: *Escherichia coli* and *Pseudomonas aeruginosa* (Gram-negative) and *Bacillus subtilis* and *Lactobacillus fermentum* (Gram-positive). The antimicrobial assays performed in saline media revealed that SA-LNPs were selectively toxic to Gram-positive bacteria, and no significant antimicrobial effects were found against the Gram-negative strains. Time-kill experiments showed that 25 μg mL^{-1} SA-LNPs were able to inactivate more than 90% of the Gram-positive bacteria after 30 min exposure. We conducted *in vitro* and *in vivo* assays to evaluate the production of reactive oxidative species (ROS), such as glutathione and 2′,7′-dichlorodihydrofluorescein diacetate (H_2DCFA). These assays indicated that oxidative stress was not the underlying mechanism involved in the antimicrobial activity of SA-LNPs. This finding corroborates that SA-LNPs could scavenge radicals of 2,2-diphenyl-1-(2,4,6-trinitrophenyl)hydrazin-1-yl (DPPH), confirming their strong antioxidant property. Although direct oxidative stress was ruled out as the probable mechanism of action, we still cannot dismiss an indirect pro-oxidant effect resulting from the SA-LNPs-containing adsorbed ROS coming into direct contact with the cell wall.

Received 2nd November 2023
Accepted 19th December 2023

DOI: 10.1039/d3su00400g

rsc.li/rscsus

Sustainability spotlight

Effective management of bacterial growth is a crucial requirement across various industries, including food, medicine, agriculture, and engineering. As the need to prevent bacteria proliferation increases, there is a need for the development of antimicrobial materials that can inactivate bacteria without contributing to the development of antibiotic-resistant microorganisms. Many nanomaterials, such as graphene oxide and metallic nanoparticles require either harsh chemical conditions or expensive and naturally depleting chemical precursors for their synthesis. Metallic nanoparticles, such as silver, also leach toxic ions that pose toxicological risks to living organisms in the aquatic environment, limiting the scope of their application. As a result, there is a high demand for low-cost, non-leaching, and antimicrobial nanomaterials made from renewable and naturally abundant feedstocks. To meet this pressing demand, we extracted lignin from a plant-based resource using simplified acid-alkaline pre-treatments. We then converted the pure extracted lignin into nanoparticles (LNPs) through a straightforward self-assembly (SA) method. The resulting SA-LNPs have a negatively charged surface and an average size of about 84 nm. Standard antimicrobial assays show that the SA-LNPs are selectively toxic to Gram-positive bacteria, making them a highly sustainable material with a broad range of potential applications, including water sanitation, controlling microbial proliferation in food packing, and developing anti-biofouling surfaces. Our work follows the principles of the UN sustainable development goals: clean water and sanitation (SDG 6), industry, innovation, and infrastructure (SDG 9), and sustainable consumption and production patterns (SDG 12).

[a]*Engineering School of Sustainable Infrastructure & Environment, Department of Environmental Engineering Sciences, University of Florida, Gainesville, FL, 32611-6540, USA. E-mail: andreia.faria@essie.ufl.edu; Tel: +352-392-7104*

[b]*Department of Agribusiness, Food and Nutrition, University of São Paulo – USP, Piracicaba, São Paulo, Brazil*

[c]*Departamento de Físico-Química, Instituto de Química, Universidade Estadual de Campinas (UNICAMP), PO Box 6154, 13083-970, Campinas, São Paulo, Brazil*

[d]*School of Fine Arts, Federal University of Minas Gerais – UFMG, Belo Horizonte, MG, 31270-901, Brazil*

[e]*Department of Agroindustrial Technology and Rural Socioeconomics, Federal University of São Carlos – UFSCar, Araras, São Paulo, Brazil*

† Electronic supplementary information (ESI) available: Zeta potential and number-weighted average hydrodynamic diameters of SA-LNPs dispersed in water and saline solution; ATR-FTIR spectra of dried bulk alkaline lignin and SA-LNPs; DPPH radical scavenging activity measured for bulk alkaline lignin dissolved; SEM image of *L. fermentum* cells exposed to SA-LNPs. See DOI: https://doi.org/10.1039/d3su00400g

Introduction

Lignin is considered one of the most abundant agro-industrial byproducts on Earth, constituting 15–40% of the dry weight of lignocellulosic biomasses, such as wood and grasses.[1] It consists of crosslinked polyphenolic structures that promote plant structural integrity, rigidity, and antimicrobial properties, vital for cell wall growth.[2] The worldwide lignin market reached around USD 1.04 billion in 2022, with an expected compound annual growth rate (CAGR) of 4.9% from 2023 to 2030.[2] Lignin has been historically considered a byproduct of pulp and paper processing,[3] but the potential use of this aromatic biomacromolecule as a versatile resource for developing value-added materials, such as surfactants,[4,5] antioxidant additives,[6,7] and nanoparticles,[8,9] has been revealed by advancements in green chemistry and materials science.[10,11]

The chemical structure and composition of native lignin can differ significantly depending on the plant's taxonomy and maturation stage, cell type, and environmental factors, such as temperature and illumination conditions.[12] The ratio of monolignol-derived units, *i.e.*, guaiacyl, syringyl, and *p*-hydroxyphenyl units, also differs in softwood, hardwood, and grasses.[13] The extraction method is another variable influencing the structure of technical lignins, leading to changes in molecular weight, fragmentation pathway, and surface chemistry.[14] Although extracted lignin is usually insoluble in water at neutral and acidic pH,[15] it possesses unique antioxidant and ultraviolet-absorbance properties.[8,16] In response to the growing demand for sustainable materials, researchers are currently exploring these properties to design lignin nanoparticles (LNPs) that can be used in a wide range of applications, including drug delivery,[17] catalysis,[18] and antimicrobial therapies.[19]

LNPs are dispersible in water and exhibit inherent biocompatibility and a high surface area.[8] Such characteristics, which potentially enhance the intrinsic properties of bulk lignin, have endowed LNPs with the ability to protect against ultraviolet radiation (UV), act as antioxidants, exhibit antibacterial properties, and treat wastewater for bacterial removal.[20] Specifically, there has been a demand for low-cost and sustainable antimicrobials to combat biofilm in the marine and food industries and for the fabrication of antibacterial surfaces for textile, medical, and aerospace applications. Amidst this pressing challenge, LNPs have gained remarkable attention as a promising candidate for combating microbial proliferation while embracing sustainability principles.[21–23] Different methods have been used to prepare LNPs of varying sizes and morphologies, including solvent exchange, nanoprecipitation, self-assembly, acid precipitation, and ultrasonication.[24] For instance, spherical LNPs produced by dissolving pristine alkali lignin into ethylene glycol under acidic conditions have been found to be effective antibacterial agents against phytopathogenic Gram-negative bacteria, such as *Pseudomonas syringae* pv tomato (CFBP 1323), *Xanthomonas axonopodis* pv *vesicatoria* (CFBP 3274), and *Xanthomonas arboricola* pv *pruni* (CFBP 3894).[25] Previous studies have also combined LNPs with polymers or other nanomaterials to yield antimicrobial agents based on lignin. Binary and ternary poly(L-lactide) (PLLA)-based materials containing LNPs and different metal oxide nanoparticles, such as titanium oxide (TiO_2), tungsten(VI) oxide (WO_3), and silver oxide (Ag_2O), showed greater antibacterial activity against *S. aureus* than against *E. coli*.[26]

Despite the existing effort to investigate the antimicrobial activity of lignin-based nanomaterials, there have been limited studies dedicated to understanding the mechanisms of action underlying the toxicity of LNPs to bacterial cells. Slavin and co-authors were the first to conduct an integrated investigation that included physicochemical characterization, antimicrobial activity, specifying the minimum inhibitory concentration (MIC), and impacts on gene expression of bacteria exposed to silver-LNPs (AgLNPs) hybrid materials.[27] AgLNPs were tested against a panel of Gram-positive and Gram-negative multidrug-resistant (MDR) clinical bacterial isolates, including *S. aureus*, *Staphylococcus epidermidis*, *Pseudomonas aeruginosa*, *Klebsiella pneumoniae*, and *Acinetobacter baumannii*, and a variety of American Type Culture Collection (ATCC) bacterial strains. This study has successfully demonstrated the broad antibacterial efficacy of AgLNPs against Gram-positive and Gram-negative MDR and ATCC bacteria. Additionally, the study has brought to light the potential of utilizing this lignin-based hybrid nanomaterial as an efficient tool to combat microbial infections and inflammatory responses simultaneously.

In this manuscript, we propose to investigate the toxicity of LNPs to Gram-positive and Gram-negative bacteria models utilizing a straightforward self-assembling (SA) methodology to produce water-dispersible LNPs. We recovered lignin from elephant grass, a highly productive perennial grass, commonly utilized for cattle feed in the tropical regions. Pure lignin was isolated through acid precipitation from an alkaline liquor remaining after a sequential acid-alkaline pretreatment applied to elephant grass leaves. Lignin was self-assembled (SA) into LNPs through the solvent–antisolvent route. The self-assembled LNPs (SA-LNPs) were characterized in terms of morphology, physicochemical fingerprint, and colloidal stability in aqueous dispersions, then tested against four ATCC bacterial strains, *i.e.*, *Bacillus subtilis*, *Lactobacillus fermentum*, *Escherichia coli*, and *P. aeruginosa*. Our findings suggest a concentration-dependent toxicity of SA-LNPs to Gram-positive bacteria, while no antibacterial effect was observed against the Gram-negative ones. The present study is significant as it explores the potential application of SA-LNPs as sustainable and eco-friendly alternative antimicrobial agents while shedding light on its possible mechanisms of action through oxidative stress and free radical scavenging assays. This promising approach aligns with the principles of green chemistry and sustainability, exhibiting a significant scope for developing novel strategies in the realm of antimicrobial research.

Experimental section

Materials and chemicals

Sodium chloride (NaCl – Crystalline/Certified ACS), LB Broth Miller, Agar (Powder/Flakes), sodium phosphate dibasic (anhydrous, certified ACS), ethanol (absolute, 200 proof,

Molecular Biology Grade), tris(hydroxymethyl)aminomethane hydrochloride (Tris–HCl, 99%), sodium bicarbonate, and hydrogen peroxide (H_2O_2, 30–32%) were obtained from Fisher Scientific. De Man–Rogosa–Sharpe media (MRS) was acquired from Becton-Dickinson (Franklin Lakes, NJ, USA). Glutaraldehyde (50% aqueous solution, Electron Microscopy Grade), paraformaldehyde (16% aqueous solution, Electron Microscopy Grade), and hexamethyldisilazane (>97.0%) were obtained from Electron Microscopy Sciences (Hatfield, PA, USA). Glutathione (98%) was obtained from Acros Organics. 5,5′-Dithiobis (2-nitrobenzoic acid) (DNTB or Ellman's reagent, 99%) was acquired from Alfa Aesar. Sulfuric acid (H_2SO_4, 98%), sodium hydroxide (NaOH, certified ACS), acetone (certified ACS), 1,4-dioxane (certified ACS), and methanol (certified ACS) were obtained from Synth (Diadema, SP, Brazil). Uranyl acetate (>99%) was acquired from Fluke Chemie AG (Buchs, Switzerland). 2,2-diphenyl-1-(2,4,6-trinitrophenyl)hydrazin-1-yl (DPPH radical) was purchased from Sigma-Aldrich (St. Louis, MO, USA). Unless otherwise specified, all chemicals were dissolved in deionized (DI) water with a resistance of 18.2 MΩ cm obtained from a Milli-Q® Direct Water Purification System (EMD Millipore, Burlington, MA, USA).

Isolation of bulk alkaline lignin and production of self-assembled lignin nanoparticles (SA-LNPs)

Lignin was extracted from elephant grass (*Pennisetum purpureum*) after a sequential acid-alkaline pretreatment (Fig. 1). Plants with approximately one year of growth were harvested at the Institute of Animal Science and Pastures (Nova Odessa, Brazil). Leaves were separated, dried at 60 °C for 24 h in an oven with air circulation (Tecnal TE-394/3, Piracicaba, Brazil), then knife milled in a grinder equipped with a 10-mesh sieve (SOLAB – SL 31, Piracicaba, Brazil). Milled leaves were treated with 1% (v/v) H_2SO_4 and a subsequent step with 2% (w/v) NaOH at 121 °C and 1.05 bar for 40 minutes in an autoclave (Phoenix AV-75, Araraquara, Brazil).[28] In the acid stage of the process, a solid-to-liquid ratio of 1 : 10 (grams of biomass per milliliter of solution) was employed to remove hemicellulose effectively. A 1 : 20 solid-to-liquid ratio was utilized in the subsequent alkaline step to extract a relatively pure and lignin-rich fraction. The alkaline liquor was then acidified by adding concentrated H_2SO_4 dropwise under constant magnetic stirring (at 400 rpm) until pH reached 2. This resulted in the precipitation of large particles of bulk lignin. The ensuing precipitate was thoroughly

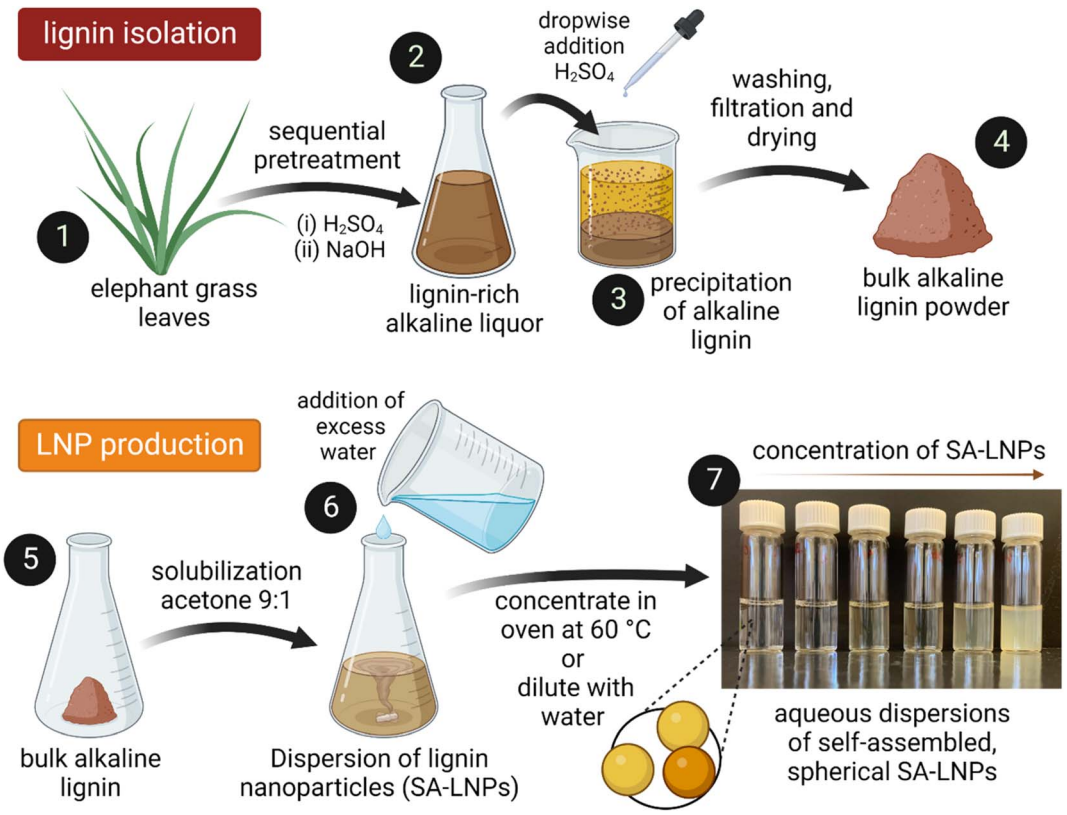

Fig. 1 Illustration of lignin extraction from elephant grass leaves and its conversion into nanoparticles. The process initiates by milling the elephant grass leaves (1), followed by sequential treatment with dilute acid and alkali to produce a lignin-rich alkaline liquor (2). A few drops of concentrated sulfuric acid is added to the alkaline solution, leading to the precipitation of alkaline lignin (3). The resulting lignin then undergoes washing, filtering, and drying processes, which yield purified and bulk lignin powder (4). The next step involves dissolving the powder in a mixture of acetone at a 9 : 1 ratio (5), followed by the addition of excess deionized water to the solution (6). This step results in the formation of aqueous dispersions of spherical SA-LNPs. These nanoparticles can either be concentrated in an oven or diluted with water, as evidenced by the photos captured under visible light (7). The concentration of nanoparticles in the media has a direct impact on the color and opacity of the SA-LNPs in aqueous dispersions. Created with https://BioRender.com.

rinsed by vacuum filtering until pH reached a range of 6–7. Finally, the solid material, the alkaline lignin, was dried in an oven at 40 °C for 12 hours.

A solvent–antisolvent approach was used to produce the LNPs, employing the methodology presented by Camargos & Rezende[28] as depicted in Fig. 1. Initially, 0.05 g of lignin powder were dissolved in a 10 mL mixture of acetone and water at room temperature while ensuring constant stirring with a magnet at 400 rpm. Subsequently, excess DI water (990 mL) were added to the solution to generate aqueous dispersions of self-assembled LNPs (SA-LNPs). The SA-LNP dispersions were filtered under vacuum to remove large aggregates and concentrated to around 1000 μg mL^{-1} *via* evaporation in an oven at 60 °C. Finally, we stored the nanoparticles in a refrigerator at 4 °C.

Physicochemical and morphological characterization of SA-LNPs

Attenuated total reflectance-Fourier transform infrared (ATR-FTIR) spectra of bulk alkaline lignin and oven-dried (60 °C) SA-LNPs were obtained in an Agilent Cary® 630 FTIR spectrometer (Santa Clara, CA) using a spectral resolution of 4 cm^{-1} and 128 scans. The mean number-weighted hydrodynamic diameter and zeta potential of lignin nanoparticles, with a concentration of *ca.* 50 μg mL^{-1} in aqueous dispersion at pH 6–7 or in saline solution (0.85% (w/v) NaCl), were measured in a Malvern Zetasizer® Nano ZS-Zen 3600 (Malvern, UK) using standard DTS-1070 disposable folded capillary cells with a fixed 173° scattering angle for size by dynamic light scattering and 12.8° for zeta potential measurements. Data were collected every 30 minutes over 6 hours. Atomic force microscopy (AFM) topography images of dried SA-LNPs were obtained in a Shimadzu SPM 9600 microscope using non-contact mode with an NCHR probe (curvature radius of 8 nm). 10 μL of SA-LNP aqueous dispersion (10 μg mL^{-1}) were collected, deposited on mica substrates, and dried for 4 h at room temperature before the analysis. A scanning rate of 1 Hz (1 line s^{-1}) and a 512-pixel resolution were applied to obtain AFM images. Topography images were treated and analyzed using Gwyddion 2.56 software (**https://Gwyddion.net**). Transmission electron microscopy (TEM) analysis of SA-LNPs was carried out in an FEI Tecnai G2 Spirit Twin TEM (FEI Corp., Hillsboro, OR) microscope. Dispersions of nanoparticles (5–20 μg mL^{-1}) at pH 6 were deposited on 400 mesh copper grids with carbon film and dried in a desiccator for 2 hours at room temperature before analysis. At least 120 nanoparticles in 7 different TEM images were measured for each sample using ImageJ software.

Concentration-dependent toxicity of SA-LNPs in suspension

SA-LNPs were tested against four different types of bacteria: (1) two Gram-positive cells (*B. subtilis* subsp. Spizizenii (ATCC 6633)) and *L. fermentum* (ATCC 9338), and (2) two Gram-negative models (*E. coli* (ATCC 8739)), and *P. aeruginosa* (ATCC 27853). *B. subtilis*, *E. coli*, and *P. aeruginosa* were cultivated in LB (Luria–Bertani), whereas *L. fermentum* grew in MRS (De Man–Rogosa–Sharpe) broth overnight. All four bacteria models were incubated separately in an orbital shaker incubator at 200 rpm or until the optical density (600 nm) reached 1.0. *L. fermentum* was incubated at 35 °C, while the other three microorganisms were kept at 37 °C during incubation. Subsequently, cells were recovered by centrifugation and washed three times with sterile saline solution (NaCl 0.85%) (w/v) and then diluted (1 : 10) to obtain an inoculum containing ~10^8 colony-forming units per mL (CFU mL^{-1}). To determine the efficacy of nanoparticles in killing bacteria in suspension, we thoroughly evaluated their antimicrobial activity. Using Eppendorf microtubes, 0.9 mL of the SA-LNPs dispersion were mixed with 100 μL of the bacteria suspension. Before use, the SA-LNPs were diluted in a sterile saline solution and sonicated for 15 minutes. The well-dispersed SA-LNPs were added to the microtubes to reach final concentrations of 0 (control), 12.5, 25, 50, and 100 μg mL^{-1}. The tubes were then gently mixed for 3 hours at room temperature and kept away from any light sources. Once the 3 hour contact period had elapsed, aliquots of each tube were extracted, serially diluted in sterile saline solution, and plated on LB agar or MRS agar (*L. fermentum*) plates to determine whether any bacteria remained viable. The plates were incubated overnight at 37 or 35 °C (*L. fermentum*), and the antimicrobial results were expressed as a percentage of the control. The assay was conducted in triplicate.

Time-dependent toxicity of SA-LNPs

We performed time-kill experiments using a protocol established elsewhere to evaluate the antimicrobial properties of SA-LNPs over time.[5] We conducted the experiments using SA-LNPs at their MIC for Gram-positive strains *B. subtilis* and *L. fermentum*, cultivated overnight in LB and MRS agar plates, respectively. Isolated colonies of *B. subtilis* and *L. fermentum* were transferred to 30 mL fresh and sterile LB and MRS media, respectively. The microbial suspensions were incubated in an orbital shaker at 200 rpm and their respective optimal temperatures until the OD_{600} achieved values around 1.0. The cells were centrifuged and washed thoroughly with a sterile 0.85% (w/v) NaCl aqueous solution to remove excessive nutrients and media constituents. The cells were resuspended in saline to reach a final concentration of ~10^8 cells per mL. At their MIC, 100 μL of this bacterial suspension was added to 2.0 mL microtubes containing 900 μL of the SA-LNPs. Tubes containing the bacteria cells without the SA-LNPs was used as controls. The microtubes were incubated at room temperature under mild rotational speed (~60 rpm). A 100 μL aliquot of each microtube was withdrawn at different incubation times (0, 15 min, 30 min, and 1, 2, and 3 h), serial diluted in saline solution, and then plated on LB or MRS agar. The plates followed incubation at the respective optimum temperatures for each bacteria strain. Bacterial concentration was then calculated after colony counting. All the tests were carried out in triplicate.

Morphological characterization of bacteria cells after exposure to SA-LNPs

SEM images of bacteria cells were acquired to evaluate the morphological characteristics of the cells after 3 hour exposure to the SA-LNPs. *B. subtilis* and *L. fermentum* cells contacted 25 μg mL^{-1} suspensions of SA-LNPs for 3 hours under room

temperature and ~60 rpm rotational shaking. Following incubation, the assay suspension, including the control samples, was filtered through a 0.22 μm PVDF filter. The same procedure was performed for the control samples, consisting of cells suspended in saline solution without nanoparticle addition. The cells retained by the filters were washed with 0.2 M Sorenson's buffer (pH 7.2) and fixed using a Karnovsky's fixative solution (2.5% glutaraldehyde and 2% paraformaldehyde diluted in 0.2 M Sorenson's buffer, pH 7.2) for 3 hours. After removing the fixative solution, the cells were rinsed with 0.2 M Sorenson's buffer (pH 7.2), deionized water, and exposed to a series of aqueous ethanol solutions for dehydration. This step includes sequentially immersing filters in aqueous ethanol solutions of 50, 70, 80, 90, and 100% (v/v) for 10 min per solution, initiating with the most diluted solution and finalizing with the most concentrated (absolute ethanol). Filters were then immersed in hexamethyldisilazane (HMDS, 97.0%) for 10 min and dried in a desiccator overnight at room temperature. Filters containing the fixed cells were carefully mounted on standard SEM stubs using double-sided carbon tape and sputter-coated with gold-palladium in a Denton Desk V Sputter Coater. Cells were imaged in a Hitachi SU5000 Schottky Field-Emission SEM operating at an accelerating voltage of 5 kV.

Assessing the oxidative properties effect of SA-LNPs

We determined the potential oxidative effect of SA-LNPs by testing their ability to oxidize glutathione (GSH) *in vitro*.[29–33] GSH is a well-known antioxidant in biological systems[34,35] and its oxidation indicates the potential oxidative effect of the LNPs. 20 μL of a GSH solution (100 mM) were mixed with 600 μL of bicarbonate buffer (0.5 M, pH 8.6), which were then added to a 5.98 mL aliquot of SA-LNPs dispersions (200 μg mL^{-1}). The final concentration of GSH is to reach 4 mM. The samples were placed on an orbital shaker, protected from light, for 3 hours at room temperature. After the contact time, an aliquot of 900 μL of each sample was mixed with 30 μL of a 100 mM Ellman's reagent (ethanol solution) and 1570 μL of Tris–HCl buffer (1 M, pH 8.3). Aliquots of 1 mL were collected, filtered through a 0.45 μm syringe filter, and submitted to absorption reading at 412 nm in a spectrophotometer (Hitachi U-2900, Japan), using a path length of 1 cm and an extinction coefficient of 14 150 M^{-1} cm^{-1}. The oxidation of GSH by H_2O_2 was used as a positive control, and a solution using deionized water without SA-LNPs was used as a negative control. The loss of GSH was determined and reported as a percentage by comparing the percentage loss of GSH to the control.

A 2′,7′-dichlorodihydrofluorescein diacetate (H_2DCFDA) assay was carried out to investigate the potential impact of SA-LNPs on forming reactive oxygen species (ROS) in bacterial cells.[29,30,36] Unlike the glutathione assay that probes the formation of ROS in an abiotic condition, the H_2DCFDA method is performed *in vivo*. It indirectly detects intracellular ROS levels in cells before and after exposure to the SA-LNPs. A bacterial suspension (1.9 mL) containing 10^8 CFU mL^{-1} was mixed with 100 μL of SA-LNPs stock solutions to obtain a final 200 μg mL^{-1} concentration. The mixture was then incubated for 3 hours at room temperature with mild agitation (60 rpm). Following this, 10 μL of H_2DCFDA solution (10 mM, dissolved in DMSO) was added to 2 mL of the bacteria-LNPs suspension, and the samples were incubated for 15 minutes, protected from light. Fluorescence intensity measurements were taken using a microplate reader (Cytation 5 imaging reader, Biotek Instruments, Vermont, USA) with an excitation wavelength of 495 nm and fluorescence emission collected at 527 nm. Menadione was used as a positive control for ROS generation, and the fluorescence intensity was normalized to the control samples without LNPs.

Assessing the antioxidant properties of alkaline lignin and SA-LNPs

The DPPH radical scavenging activity of bulk alkaline lignin in dioxane solution and SA-LNPs in aqueous dispersions (deionized water or 0.85% (m/v) NaCl) was evaluated using a colorimetric method by UV-Vis spectroscopy. The methodology was based on the approach reported by Camargos & Rezende.[28] To conduct the experiment, DPPH dissolved in methanol (2 mL, 65 μmol L^{-1}) was added to (a) bulk alkaline lignin solution in 90% (v/v) dioxane (1 mL, 150 μg mL^{-1}), (b) SA-LNP dispersion in deionized water (1 mL, 150 μg mL^{-1}), or (c) SA-LNPs dispersion in saline solution (1 mL, 150 μg mL^{-1}). Controls were also prepared to contain DPPH radical solution (2 mL, 65 μmol L^{-1}) added to (a) 90% (v/v) dioxane (1 mL), (b) deionized water (1 mL), or (c) saline solution (1 mL). The background for all measurements contained equivalent amounts of (a) methanol and dioxane, (b) methanol and deionized water, (c) methanol and saline. The relative intensity of the absorption band at 520 nm (λ_{max}) of the UV-Vis spectra collected at time 0, 16, and 30 minutes in a Cary 50 Agilent spectrophotometer was used to analyze the concentration of DPPH radical. The scavenging activity was calculated as follows (eqn (1)):

$$\text{Scavenging activity}(\%) = \frac{(\text{absorbance control at 520 nm}) - (\text{absorbance sample at 520 nm})}{(\text{absorbance control at 520 nm})} \times 100 \quad (1)$$

Results and discussion

Physicochemical and morphological properties of self-assembled lignin nanoparticles (SA-LNPs)

Lignin was extracted from elephant grass leaves using a sequential acid-alkaline pretreatment process, resulting in

a sample with a purity of approximately 98% and an average molecular weight of 6932 ± 37 g mol^{-1}.[28] The extracted lignin appeared as a brown-to-black powder soluble in alkaline aqueous media and organic solvents such as acetone and dioxane. Due to its solubility behavior and the amphiphilic nature of its macromolecules, the extracted lignin was used as a precursor for obtaining lignin nanoparticles *via* a self-assembly method using acetone as a solvent and water as an antisolvent,[28,37] as depicted in Fig. 1.

When water is added to lignin dissolved in acetone, the lignin macromolecules wrap around themselves, forming small spheres approximately 80 nm in diameter (Fig. 2D). The morphology and average size of the SA-LNPs are demonstrated by TEM and AFM imaging (Fig. 2A–C). TEM micrographs (Fig. 2A and B) revealed the presence of holes on the surface of certain hollow nanospheres. This characteristic is likely attributed to the analysis conditions, as the solvent (water/acetone) that was initially trapped within the nanoparticle core evaporates and disrupts the morphology under high vacuum, sufficiently elevated temperature, and voltage of the TEM analysis.[8] No holes are observed in AFM micrographs (Fig. 2C), as this image was acquired under ambient conditions. The more hydrophobic parts of the lignin molecules tend to associate and hide in the inner part of the sphere through non-covalent interactions such as hydrogen bonding and pi-stacking. In contrast, the hydroxyl and carboxyl functional groups are exposed in the outer shell of the SA-LNPs dispersed in water. This results in stable, spherical-like nanoparticles that exhibit outstanding colloidal stability, with a zeta potential of −36 ± 1 mV in freshly prepared aqueous dispersion at pH 6–7. The negative zeta potential indicates an adequate electrical double-layer repulsion mechanism that ensures the stability of the nanoparticles in water. The zeta potential and number-weighted average hydrodynamic diameter of the SA-LNPs in water remained constant for up to 6 hours after preparing the nanoparticles. The average values were −29 ± 4 mV and 94 ± 9 nm, respectively, as shown in Fig. S1.† However, when the SA-LNPs

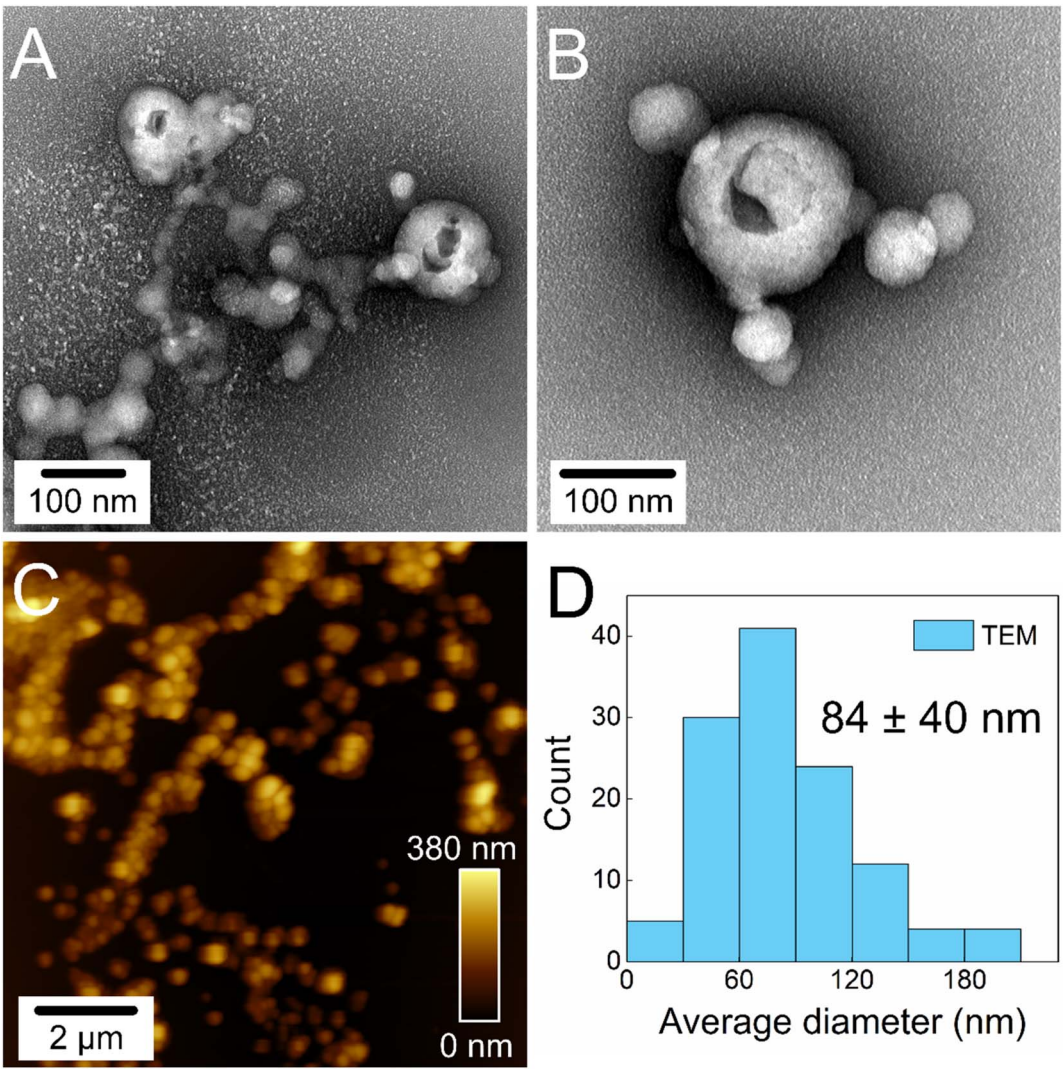

Fig. 2 (A and B) TEM images of SA-LNPs. (C) AFM topography images of SA-LNPs. (D) Size distribution histogram of the average diameter of lignin nanoparticles obtained through measurements *via* TEM images using the software ImageJ.

were dispersed in saline solution (0.85% NaCl), the standard medium for the antimicrobial assay, there was a slight decrease in the colloidal stability over time. The zeta potential modulus was reduced to -24 ± 1 mV and remained stable for 6 hours, with a cumulative average of -19 ± 3 mV (Fig. S1A†). This increased the number-weighted average hydrodynamic diameter of the SA-LNPs from 94 ± 9 nm to 142 ± 71 nm (Fig. S1B†).

The chemical structure of alkaline lignin and SA-LNPs was analyzed using ATR-FTIR. The FTIR results presented in Fig. S2† reveal the presence of typical absorption bands related to the functional groups of lignin in both the bulk precursor and dried nanoparticles. However, the relative intensity of these bands is slightly lower in the SA-LNPs. These similar spectra confirm that most of the structural features of lignin are retained by SA-LNPs. The 2920 and 2850 cm^{-1} bands are assigned to C–H stretching in methoxyl groups.[38] The multiple bands in the 1420–1590 cm^{-1} range can be attributed to C=C stretching in aromatic rings.[38] Additionally, the bands at 1215, 1116, and 1028 cm^{-1} correspond, respectively, to C–O aryl-ether groups, C=O stretching, and aromatic C–H in-plane deformation.[39]

SA-LNPs show selective toxicity to Gram-positive cells

We conducted a study to examine the antimicrobial properties of SA-LNPs. We tested the nanoparticles on two Gram-negative bacteria (*E. coli* and *P. aeruginosa*) and two models of Gram-positive bacteria (*B. subtilis* and *L. fermentum*) in suspension, as shown in Fig. 3A–D. The tests, using concentrations of 0, 12.5, 25, 50, and 100 μg mL^{-1}, revealed that SA-LNPs had minimal to no toxicity to both models of Gram-negative bacteria (*E. coli* and *P. aeruginosa*) (Fig. 3A and B). Even at higher concentrations (100 μg mL^{-1}), we could not observe any significant inhibition of *E. coli* or *P. aeruginosa* cells by the lignin nanoparticles. Exposure to the SA-LNPs caused *E. coli* cells to grow (Fig. 3A). This suggests that the cells could have used the SA-LNPs as a nutrient source or growth promoters. We make this observation based on the antimicrobial assay being performed in saline solution (NaCl, 0.9% w/v) without

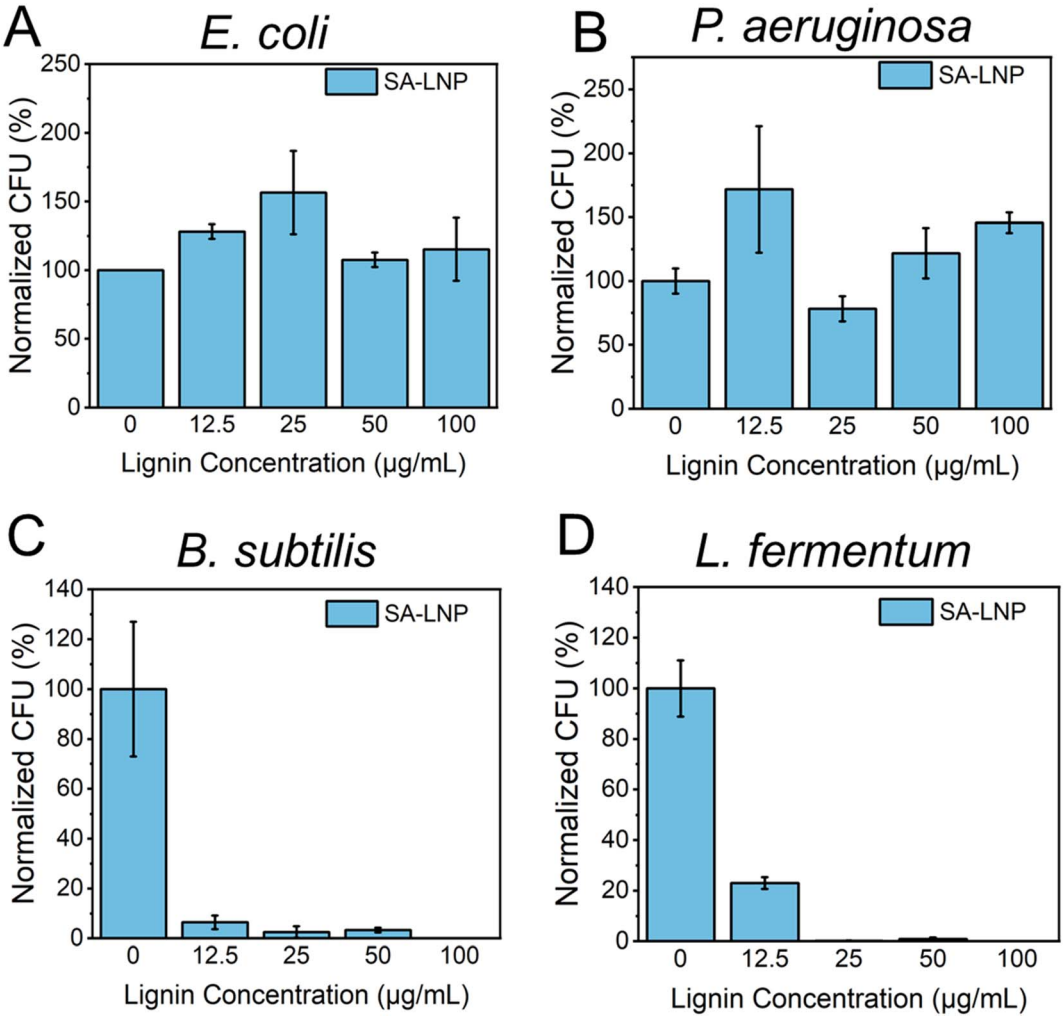

Fig. 3 Antimicrobial properties of self-assembled lignin nanoparticles (SA-LNPs) against Gram-negative (A) *E. coli* and (B) *P. aeruginosa* and Gram-positive (C) *B. subtilis* and (D) *L. fermentum*. The bacteria cells were exposed to SA-LNPs in a saline solution for 3 hours. Cell viability was measured using a plate counting assay. The results were analyzed and expressed as a percentage reduction in colony-forming units (CFU).

supplementary organic or inorganic nutrients. We also noticed a similar effect of cellular growth for *P. aeruginosa* cells when they contacted the SA-LNPs at all concentrations except for 25 μg mL^{-1}, where the cells were inhibited by ~30–40% compared to a control sample without the SA-LNPs (Fig. 3B). Since neither SA-LNPs showed toxicity to *E. coli* or *P. aeruginosa* at the tested concentrations, we could not estimate the MIC for these two Gram-negative models.

On the other hand, Fig. 3C and D demonstrated that the SA-LNPs were highly toxic to both models of Gram-positive bacteria (*B. subtilis* and *L. fermentum*) at all concentrations investigated. Even concentrations as low as 12.5 μg mL^{-1} were enough to inactivate *B. subtilis* cells by nearly 90% compared to the negative control (Fig. 3C). Similarly, *L. fermentum* cells were inhibited by almost 80% at 12.5 μg mL^{-1} (Fig. 3D). Therefore, the concentrations of SA-LNPs above 12.5 μg mL^{-1} were highly toxic to both Gram-positive bacteria in aqueous media. We observed inhibition above 90% for *B. subtilis* at 25 and 50 μg mL^{-1} concentrations of SA-LNPs. *L. fermentum*, however, seemed more sensitive to higher concentrations of the SA-LNPs than *B. subtilis*. The inactivation of *L. fermentum* achieved almost 100% at the concentration of 25 μg mL^{-1} of SA-LNPs (Fig. 3D). At the 100 μg mL^{-1} concentration, the SA-LNPs were very toxic to both *B. subtilis* and *L. fermentum* cells, and no bacteria colonies were observed on the agar plates after the 3 hour exposure to the nanoparticles. Remarkably, the plant-derived nanomaterial acted without the assistance of antibiotics or toxicity enhancers such as copper and silver nanoparticles.

Our analysis of Fig. 3B and D leads us to conclude that the toxicity of SA-LNPs depends on the concentration of the nanoparticles and the strain type. The minimum inhibitory concentration (MIC) required for complete inactivation of *B. subtilis* was considered to be 25 μg mL^{-1} for both *B. subtilis* and *L. fermentum* as SA-LNPs demonstrated excellent antimicrobial activity against the Gram-positive bacteria at this low concentration. This level of toxicity is like that of metallic nanoparticles, such as silver nanoparticles (AgNPs), which typically have MICs around 6–20 μg mL^{-1}. Considering the antimicrobial assays performed in suspension, SA-LNPs improved antimicrobial properties compared to cellulose nanocrystals[29] or graphene oxide.[31,32,40] For instance, pristine graphene oxide (GO) sheets exhibit low toxicity to bacteria in water suspensions, with a MIC of around 150–300 μg mL^{-1},[40,41] which is approximately 5–10 times greater than the MIC observed for SA-LNPs in this study.

Limited studies have explored the antimicrobial properties and mechanisms of action of LNPs.[38,42–45] For example, photoactive porphyrin-encapsulated acetylated lignin nanoparticles (THHP@ActLig) exhibited antibacterial activity.[42] When exposed to white light at a dose of 4.16 J cm^{-2}, THHP@ActLig deactivated 99.999% of Gram-positive bacteria (*Staphylococcus aureus*, *Staphylococcus epidermidis*, and *Enterococcus faecalis*). THHP@ActLig also affected Gram-negative bacteria, particularly *P. aeruginosa*, in a concentration-dependent manner. However, *E. coli* was resistant to the toxic effects of THHP@ActLig at all tested concentrations, whereas *P. aeruginosa* was sensitive at concentrations of 10 μM under dark and light exposure conditions. It is essential to note that THHP@ActLig particles are infused with porphyrin, which is a photodynamic compound generating oxidative reactive species (ROS) in the form of singlet oxygen, resulting in the toxicity of THHP@ActLig. Contrary to our findings that show excellent antimicrobial properties for pristine SA-LNPs, no evidence of toxicity was reported for AcLig without including porphyrin.

Previously, a recent study investigated the effectiveness of treating alkali lignin with acidic conditions before turning it into LNPs with different sizes and surface chemistries.[43] The LNPs showed unique inhibition halos (zones of suppression of microbial growth surrounding an antimicrobial agent) against common plant pathogens such as *Pseudomonas syringae pv tomato*, *Xanthomonas axonopodis* pv *vesicatoria (Xav)*, and *Xanthomonas arboricola* pv *pruni (Xap)*. The study also assessed the antibacterial activity of the LNPs by examining bacterial growth in broth media. Notably, the results showed that *Xap* was the most susceptible pathogen to the LNPs, with a 3-log unit reduction in cell availability observed after exposing it to 4% wt LNPs suspensions for 24 hours. It is essential to highlight that the lignin utilized in this study was a pure commercially graded Sigma-Aldrich alkali lignin rather than the lignin extracted from a grass feedstock, as featured in this manuscript. Additionally, the concentration of LNPs showing toxicity (4% wt) was significantly higher than that reported here for SA-LNPs (12.5–100 μg mL^{-1}). Unfortunately, the authors did not further investigate the impact of different LNP concentrations on the target microorganisms.

Recent research has demonstrated the antibacterial activity of phenolated lignin nanoparticles (Phe-LigNPs). These nanoparticles are produced by grafting polyphenol tannic acid into lignin and then subjecting it to high-intensity ultrasound.[45] The PheLigNPs effectively combat Gram-positive *S. aureus* and *B. cereus* at a concentration of 1.25 mg mL^{-1}, and Gram-negative *P. aeruginosa* and *E. coli* at 2.50 mg mL^{-1}. The reduction in cell availability accompanied a reduction in metabolic activity measured by the transformation of blue resazurin into its reduced pink form by the bacterial respiratory chain. Unlike our results, the PheLigNPs inactivated both Gram-positive and Gram-negative cells, although their effect was more pronounced against the Gram-positive bacteria. The SA-LNPs were ten to fifty times more toxic than PheLigNPs, with MICs of 25–100 μg mL^{-1}, thus revealing the superior toxicity of the grass-derived SA-LNPs to Gram-positive bacteria. Meanwhile, kraft lignin nanospheres showed toxicity to Gram-positive *Bacillus megaterium* and Gram-negative *E. coli*.[44] No significant differences in toxicities were found between the two groups of bacteria. The authors reported an IC_{50} (concentration needed to inactivate 50% of the bacterial population) of 115 μg mL^{-1} for *B. megaterium*, further enhanced to 78 μg mL^{-1} under irradiation with blue light emitting diodes (LED) (12 W).

The selective toxicity of SA-NLPs against Gram-positive bacteria is consistent with previous studies investigating the antibacterial activity of extracted lignin.[46,47] For instance, bulk lignin extracted from corn stover residue used in ethanol

production was effective in inactivating Gram-positive *Listeria monocytogenes* and *S. aureus*, while having no effect on Gram-negative *E. coli* O157:H7 and *S. enteritidis*.[48] Additionally, polymer dehydrogenate polymer (DHP) (a lignin model compound) intercalated with alginate, has shown strong antimicrobial properties to a broad range of both Gram-positive and Gram-negative microorganisms. The DHP-alginate material displayed an improved antibacterial activity against *L. monocytogenes* compared to the other bacteria tested. Another study has investigated the antimicrobial properties of 35 different polyphenols against three Gram-positive and three Gram-negative foodborne pathogenic bacteria.[49] The polyphenols have demonstrated varying toxicity depending on the bacterial strain. The authors found that *L. monocytogenes* was generally more sensitive to polyphenols, while *P. aeruginosa* was more resistant. Furthermore, the chemical modification of LNPs with noble-metal nanostructures, such as silver nanoparticles, has been investigated to enhance their antimicrobial properties.[27,50] Given the complexity of the chemical and structural composition of hybrid metal-LNP materials, this type of work will not be discussed for comparison purposes.

The toxicity of SA-LNPs to Gram-positive bacteria is time-dependent

To better comprehend the effects of SA-LNPs on bacteria availability over a designed time frame, *B. subtilis* and *L. fermentum* were exposed to the nanomaterials, and cell viability was quantified at different time intervals.[30] The Gram-positive bacteria models were subjected to SA-LNPs at their respective MIC concentrations (100 μg mL^{-1} for *B. subtilis* and 25 μg mL^{-1} for *L. fermentum*) for 3 hours. Samples were collected at six distinct time intervals, and plate counting was utilized to determine the normalized percent reduction in colonies-forming units (CFU %), as illustrated in Fig. 4.

Fig. 4A shows the effects of SA-LNP exposure on *B. subtilis* in a saline solution for 3 hours. The results indicate a significant decrease in the number of viable cells of *B. subtilis* by approximately 70% within 15 minutes. Furthermore, SA-LNPs become increasingly toxic with longer exposure times, leading to over 90% inhibition after one hour. *L. fermentum* exhibits a similar pattern but with negligible cell inhibition at 15 minutes of exposure as opposed to *B. subtilis* cells (Fig. 4B). After 30 minutes of contact time, *L. fermentum* cells become 70% inactivated, and the inactivation level increases to 90% after an hour of exposure. Although *B. subtilis* cells appear more sensitive to the toxic effects of SA-LNPs at the initial 15 min exposure, the cell inactivation practically levels out after 30 min of exposure for both microorganisms. This suggests that the SA-LNPs display similar toxicity kinetics to *B. subtilis* and *L. fermentum*.

A recent research study conducted by Yang and his team has revealed that adding LNPs to media broth can delay bacterial growth during the initial 12 hours, with some strains experiencing a decline in growth rates by 2–3 logs.[38] However, it should be noted that despite the initial inhibition, some strains exhibited regrowth after 24 hours, indicating that LNPs have limited antimicrobial properties in certain conditions.

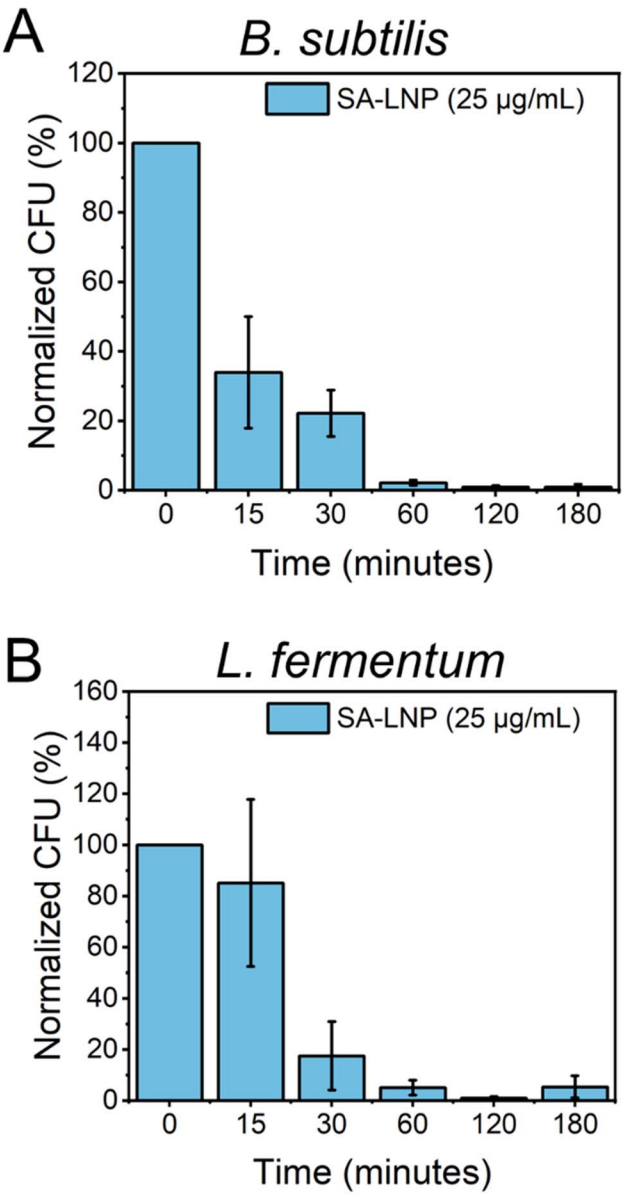

Fig. 4 Time-dependent effect of SA-LNPs (25 μg mL^{-1}) on the viability of (A) *B. subtilis* and (B) *L. fermentum* over time. Plate counting was used to determine the number of viable cells, which was expressed as the logarithm of colony-forming units (CFU). Experiments were conducted in triplicates (n = 3) and error bars represent the standard deviation.

Similarly, another study demonstrated a reduction in *P. aeruginosa*, *S. aureus*, and *B. cereus* growth when exposed to Phe-LigNPs for 24 hours.[45]

The direct production of ROS does not drive the mechanism of toxicity of the SA-LNPs

The utilization of carbon nanomaterials in the elimination of bacteria is believed to occur *via* oxidation of bacterial cells through reactive oxygen species (ROS).[31,51–53] In this study, we examine the establishment of oxidative processes through indirect and direct methods, including glutathione and

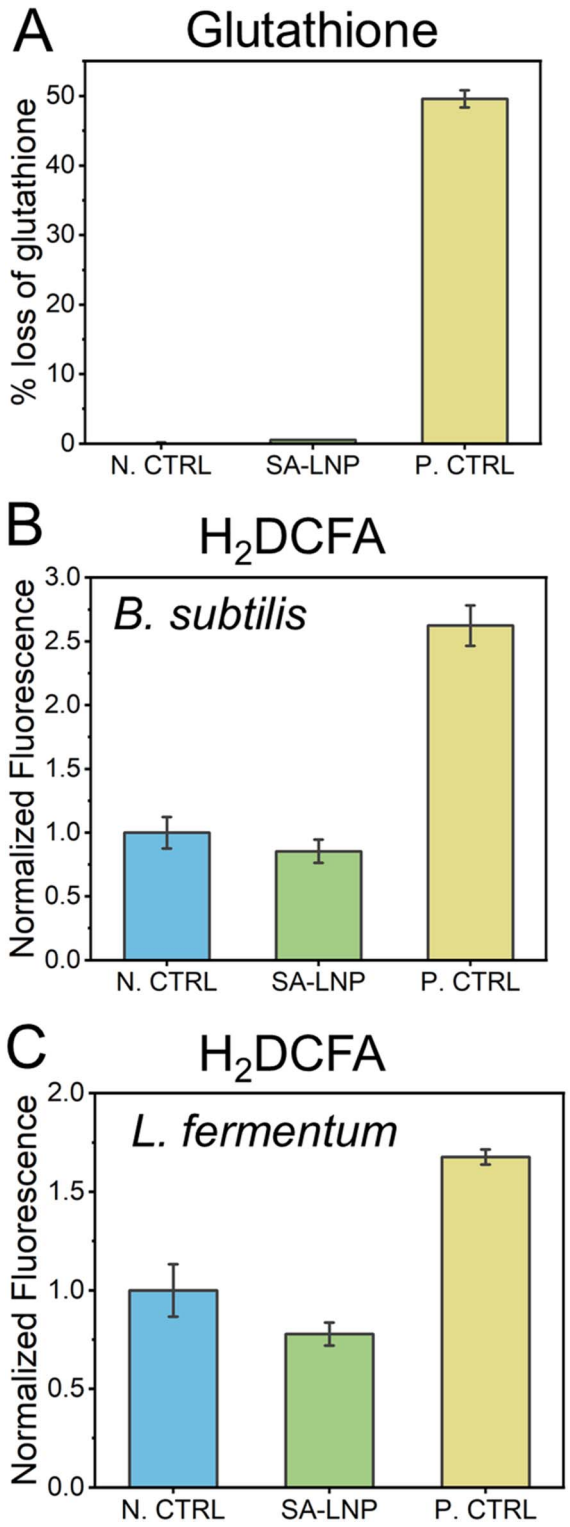

Fig. 5 (A) oxidative potential of SA-LNP *in vitro* by oxidation of glutathione. H_2O_2 was used as a positive control. H_2DCFDA method to determine the formation of reactive oxygen species (ROS) within (B) *B. subtilis* and (C) *L. fermentum* cells after exposure to SA-LNPs.

H_2DCFA assays (Fig. 5). Our findings suggest that SA-LNPs, which contain significant oxygen functionalities, may promote cellular oxidation by generating ROS.

In order to evaluate the potential of SA-LNPs to instigate oxidation through reactive oxygen species (ROS) production, a glutathione assay was conducted. Glutathione (GSH) at a concentration of 20 μM was exposed to 200 μg mL^{-1} of SA-LNPs, and the resulting measurement was taken as the loss of glutathione (Fig. 5A). The observations demonstrated that SA-LNPs have a very low propensity to induce oxidation, as there was an insignificant GSH loss. The GSH loss related to the SA-LNPs was statistically similar to the negative control (GSH without SA-LNPs). On the other hand, the positive control, H_2O_2 (10 mM), led to approximately 50% of GSH oxidation after 3 hours of exposure, thereby validating the oxidative stress assay. Based on the low levels of GSH oxidation, it can be inferred that SA-LNPs do not seem to be involved in the mechanisms of ROS generation.

To assess the accumulation of reactive oxygen species (ROS) in cells, we employed H_2DCFA, a fluorescent probe (Fig. 5B and C). Unlike the GSH assay, this test was carried out in the presence of bacteria. The probe permeates the cell wall and concentrates in the cytoplasm, where it could be oxidized if ROS is present. If H_2DCFA is oxidized, it turns into a fluorescent compound whose signal can be measured using a microplate reader.[29,30] Fig. 5B and C illustrate that bacteria treated with SA-LNPs did not display a significant difference in fluorescence compared to the control samples (bacteria without contact with SA-LNPs). However, bacteria that were exposed to H_2O_2 had fluorescence intensity almost double that of those treated with SA-LNPs. These outcomes imply no ROS accumulation inside the cells due to exposure to SA-LNPs. The GSH and H_2DCFA assays suggest that oxidative stress may not affect the toxicity of SA-LNPs to Gram-positive bacteria. Further research utilizing specific chemical probes to detect other target oxidative radicals is necessary to gain a better understanding of the participation of oxidative stress in the mechanism of toxicity.

We utilized SEM imaging techniques to evaluate the extent of surface damage inflicted upon Gram-positive cells by SA-LNPs (Fig. 6). Our investigation involved assessing the impact of exposure on both *B. subtilis* and *L. fermentum* before and after exposure. Results indicate that the morphology of the cells suffered significant damage, as depicted in Fig. 6B and D. The SA-LNPs may have induced substantial cell morphology loss, which can result in leakage of cytoplasmatic fluids. In comparison to the control group, cells treated with SA-LNPs exhibited flattened and deformed morphology. In some of the images (Fig. S3†), we can observe the deposition of SA-LNPs on the cell surface and the formation of holes on the surface of the cell wall (Fig. S3 and S4†). While SEM images cannot confirm penetration of the SA-LNPs into the cells, the particle–cell interaction observed in the SEM images (Fig. 6, S3 and S4†) may indicate a chemical affinity between the particles and the bacteria cell wall.

Similar observations were described for phenolated lignin nanoparticles (Phe-LNPs), created through the grafting of tannic acid to a commercial lignin sample (Protobind 6000) using high-intensive sonication and an enzyme mediator.[45] Upon exposure to Phe-LNPs, *E. coli* and *P. aeruginosa* cells displayed flattened shapes with multiple depressed areas. SEM

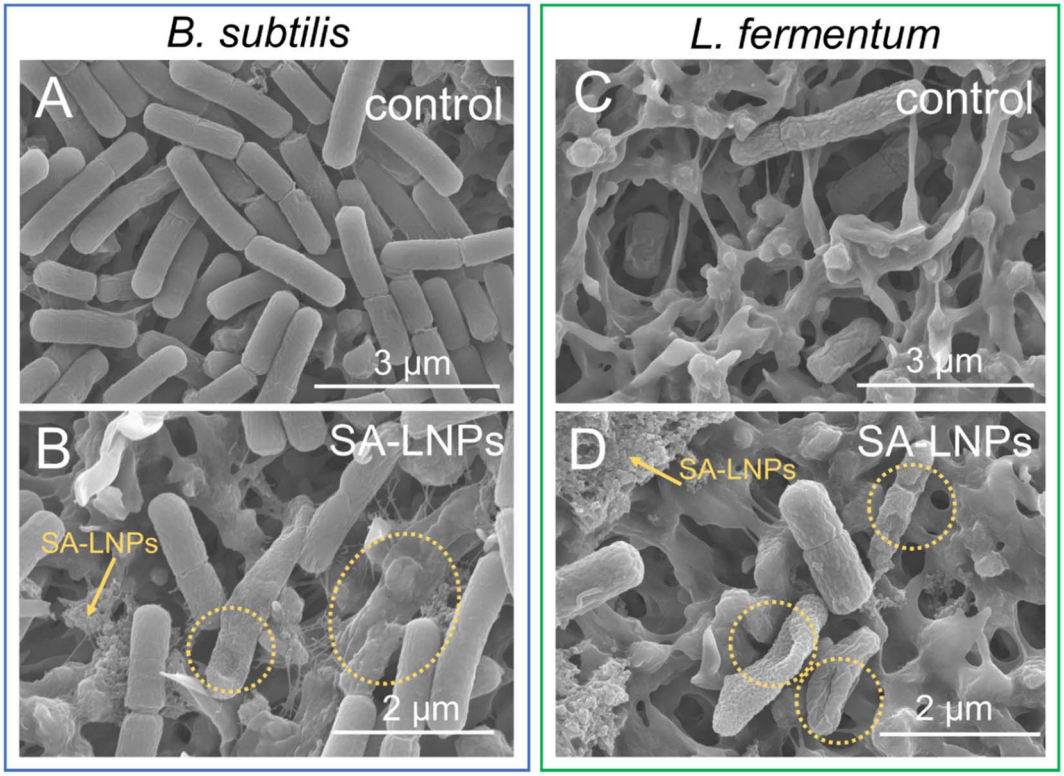

Fig. 6 SEM micrographs of *B. subtilis* (B) and *L. fermentum* (D) fixed on 0.22 μm PVDF filter after 3 hours in contact with SA-LNPs in solution. Untreated cells are denominated as control (A and C). Circles indicate morphological damage and disrupted cells, and arrows point to the presence of SA-LNPs clusters in the sample.

images suggested that SA-LNPs may cause toxicity to *B. subtilis* and *L. fermentum* by interacting with components of the cell wall of these Gram-positive cells (Fig. 6). If SA-LNPs penetrate the cell due to their small size, they can alter the pH of the cytoplasm, deactivate enzymes, and denature proteins and DNA. The size of the LNPs has been found to affect their toxicity to bacteria.[45] For instance, Phe-LNPs were more toxic to bacteria cells than bulk lignin and phenolated bulk lignin. This behavior confirms that the size of lignin-based materials is crucial to their toxicity to bacteria.

Polyphenolic compounds resembling lignin, like ferulic and gallic acids, have been shown to cause irreversible damage by changing membrane hydrophobicity and decreasing surface charge in cells of *E. coli*, *P. aeruginosa*, *S. aureus*, and *L. monocytogenes*. Such localized damages could cause membrane rupture through pore formation and the consequent release of intracellular materials, as demonstrated by increased efflux of potassium ions after exposure to the polyphenols.[54] Microorganisms exposed to phenolic compounds experience physiological alterations, such as changes in fructification bodies and abnormal production of pigments. Other studies have demonstrated that phenolic compounds composing lignin can suppress the activity of essential enzymes[55] or disturb the permeability of the cell membrane.[49,56,57]

Researchers studied the interaction between Phe-LNPs and the surface of bacteria using quartz crystal microbalance (QCM).[45] Through observation of real-time adsorption events, it was discovered that Phe-LNPs, circulating over *S. aureus* cells deposited on the sensor surface, caused a decrease in frequency and increased dissipation. These results indicated multiple interactions between the phenolic groups of the Phe-LNPs and the cell wall of the bacteria. Furthermore, evidence of membrane damage was found by staining the bacterial cells with SYTO-9 and propidium iodide. Cells with intact membranes appeared green, while those with damaged membranes appeared red. Upon incubation with the Phe-LNPs, cells appeared predominantly red, suggesting that the Phe-LNPs may have caused damage to the cell/wall membrane.[45] Together, our data and those described by Morena *et al.*[45] support a mechanism of toxicity based on the membrane-disturbing effect of the SA-LNPs. This supposed mechanism of action is also supported by quantitative structure–activity relationship (QSAR) models, whose findings suggest that the antibacterial activity of most polyphenols likely depends on the interaction of polyphenols with the cell surface.[49]

Previous studies have suggested that oxidative stress plays a role in the toxicity mechanism of LNPs.[42,45,58] However, our research on SA-LNPs indicates that they do not induce direct oxidation through the generation of ROS, as evidenced by data in Fig. 5. These findings contradict the observations made by Morena *et al.*,[45] who noted that exposure to Phe-LNPs resulted in the oxidation of H_2DCFA due to the accumulation of intracellular oxidants such as hydrogen peroxide and hydroxyl radical. In contrast, Fig. 5B and C show a lack of oxidation of

H_2DCFA and a decrease in the basal level of intracellular ROS following contact of Gram-positive cells with our SA-LNPs, thus confirming their ROS scavenger effect. This outcome is consistent with another study that demonstrated the ability of LNPs to neutralize the oxidative impact of intracellular ROS.[58]

Therefore, the damage to the cell wall (loss of surface morphology) visualized upon contact with SA-LNPs is likely associated with the interaction of the nanoparticles with the bacteria surface rather than lipid peroxidation or other disruptions caused by oxidative stress. Another study conducted by Maldonado-Carmona *et al.*[42] yielded similar results, with negligible singlet oxygen production for porphyrin-loaded LNPs in darkness, but toxicity in varying degrees observed in *P. aeruginosa* and *Salmonella epidermidis* in non-photodynamic conditions. This result also suggests that the bacteria cells were likely inactivated by a mechanism other than oxidative stress.

Research has indicated that lignin nanospray (LNSR) particles possess antimicrobial properties that are activated by light.[44] In the presence of light, bacterial cells treated with LNSR experienced a higher level of DNA leakage than those not exposed to light. However, some antibacterial effects were also noted in the absence of light, suggesting that the membrane of cells treated with LNSR may experience disruption followed by releasing intracellular materials, regardless of light exposure. These effects were found to be more pronounced under irradiation. DNA release was associated with the lipid peroxidation and ROS generation induced by the LNPs. The study did not employ indirect or direct assays to determine ROS-induced oxidative stress. As such, it is plausible that other mechanisms besides oxidative stress may be involved in the cell inactivation process by LNPs since ROS production was not quantified.

It is also plausible that the nanoparticles possess an indirect pro-oxidant effect owing to their antioxidant properties. While lignin has historically been recognized as an antioxidant, it may also exhibit pro-oxidant effects. The phenolic groups in lignin can scavenge reactive free radicals from water, leading to toxicity in microorganisms upon exposure to bacterial cells. Prior research has demonstrated a connection between the antioxidant and antimicrobial characteristics of lignin.[38,59,60] Various techniques for extracting corn stover lignin have yielded varying degrees of free radical adsorption, with the extract displaying the highest antioxidant activity, demonstrating improved toxicity to *L. monocytogenes*, *S. aureus*, and *Candida lipolytica*. Recent studies have also established positive correlations between the antioxidative properties and antibacterial activities of bulk lignin. Polyphenols can exhibit both antioxidant and pro-oxidant behaviors, as phenolic compounds can reduce metals, especially Cu(II), resulting in the generation of Cu(I) that can participate in Fenton-like reactions and produce ROS.[61] Changes in pH and the conversion of polyphenols to benzoquinones, either metabolically or otherwise, are also essential variables determining whether the behavior is antioxidant or pro-oxidant.[61]

Alkaline lignin derived from elephant grass has demonstrated antioxidant properties that are further enhanced when the lignin is converted to the nanoscale.[28] To evaluate their antiradical properties, bulk lignin, and SA-LNPs were tested for their ability to scavenge DPPH free radicals in solution. At a concentration of 50 μg mL^{-1}, solubilized bulk lignin, SA-LNPs in deionized water, and SA-LNPs in saline solution demonstrated the ability to immediately inhibit approximately 5%, 30%, and 38% of the available radicals, respectively (Fig. S5†). After 30 minutes of reaction, bulk lignin and SA-LNPs achieved up to 48% and 65–70% free radical inhibition, respectively. These results suggest a positive correlation between the antioxidant and antimicrobial properties of SA-LNPs. Positive correlations between the antioxidant and antimicrobial properties have been described in previous studies for lignin-based materials,[16,34,35] as discussed above, and other nanomaterials, such as silver nanoparticles.[62]

The effectiveness of lignin-based materials in fighting against microbes is not fully understood due to various factors, including the origin of the lignin, the techniques employed to extract and convert it into nanoparticles, and their molecular weight and surface chemistry.[63–65] Moreover, the antimicrobial activity of lignin is evaluated using different microorganisms, and there is no standardization of the type and number of microorganisms used to test its antibacterial properties. Additionally, various *in vitro* microbial assays are used to assess the toxicity of lignin, such as inhibition zones[43] and MIC[42,44] in saline solutions or growth media, which makes it challenging to compare data reliably. Furthermore, the conditions under which lignin is tested, such as exposure to irradiation or darkness,[38,42–45,66] also affect its antimicrobial properties. All these factors must be considered when analyzing the toxicity of lignin and nanolignin to bacteria cells.

Conclusion

Using an anti-solvent method, lignin extracted from elephant grass was fashioned into nanoparticles. The resulting self-assembled lignin nanoparticles (SA-LNPs) had an average size of 84 nm and retained the chemical fingerprint of aromatic rings and phenolic functional groups typical of bulk lignin. The self-assembling mechanism promotes the exposure of the hydrophilic functional groups towards the surface of SA-LNPs, imparting negative charges and high dispersibility in water to these nanostructures, which also showed enhanced antioxidant performance. We tested the antimicrobial activity of SA-LNPs in suspension against four model microorganisms, two Gram-positive (*B. subtilis* and *L. fermentum*) and two Gram-negative (*E. coli* and *P. aeruginosa*). Our results indicate that SA-LNPs have concentration-dependent toxicity to Gram-positive bacteria while showing no antibacterial effect against Gram-negative bacteria. At ~25 μg mL^{-1} concentrations, *B. subtilis* and *L. fermentum* cells were inactivated by approximately 90%. The toxic effect of SA-LNPs was observed after 15 minutes of exposure and intensified after one hour of exposure to Gram-positive cells, as indicated by the time-kill experiments. Oxidative stress assays involving glutathione and H_2DCFD confirmed that SA-LNPs did not induce ROS generation in suspension. These findings suggest that oxidative stress is not involved in

the mechanism of action of SA-LNPs against Gram-positive bacteria. It is widely understood that the thickness of the cell wall of Gram-positive bacteria is greater than that of Gram-negative bacteria. The cell wall of Gram-positive bacteria is 20–80 nm thick, while that of Gram-negative bacteria is less than 10 nm wide. Additionally, Gram-negative bacteria have an outer membrane that contains many pores and appendices. However, we presume that the chemical composition of the cell wall, rather than its thickness or structure, determines the type and strength of interactions with SA-LNPs. These interactions dictate the affinity of the SA-LNPs for the cell wall and membrane, which in turn determines the ability of these nanoparticles to cause damage to the surface of the wall/membrane and to penetrate inside the cell. Once inside, the nanoparticles can cause a range of toxic effects such as changes in cytoplasmic pH, deactivation of enzymes and proteins, and release of intracellular contents. Further research is needed to understand the extent of these chemical interactions, as well as the functional groups and chemical structures involved in these interactions and adhesion. Until the mechanism is unveiled, there is no doubt that SA-LNPs hold significant potential as antimicrobial agents for use in water treatment, active food packaging, and biomedical devices.

Author contributions

The manuscript was written through the contributions of all authors. All authors have approved the final version of the manuscript.

Conflicts of interest

The authors agree that there are no conflicts of interest to declare.

Acknowledgements

This study was financed in part by FAPESP, numbers 2018/23769-1 and 2021/12071-6, and National Council for Scientific and Technological Development (CNPq, grant number 151281/2022-0). We thank the INCT-INOMAT for providing access to AFM facility, Dr Douglas S. da Silva (*in memoriam*) for his kind technical support, the IQ-UNICAMP for providing laboratory infrastructure and access to FTIR, DLS, and UV-Vis spectrophotometer machines. The graphical abstract and Fig. 1 were created with **https://BioRender.com**.

References

1 A. J. Ragauskas, G. T. Beckham, M. J. Biddy, R. Chandra, F. Chen, M. F. Davis, B. H. Davison, R. A. Dixon, P. Gilna, M. Keller, P. Langan, A. K. Naskar, J. N. Saddler, T. J. Tschaplinski, G. A. Tuskan and C. E. Wyman, Lignin Valorization: Improving Lignin Processing in the Biorefinery, *Science*, 1979, **2014**(6185), 344, DOI: **10.1126/SCIENCE.1246843**.

2 *Lignin Market Size, Share & Trends Analysis Report, 2030*, **https://www.grandviewresearch.com/industry-analysis/lignin-market**, (accessed 2023-10-04).

3 A. Tribot, G. Amer, M. Abdou Alio, H. de Baynast, C. Delattre, A. Pons, J. D. Mathias, J. M. Callois, C. Vial, P. Michaud and C. G. Dussap, Wood-Lignin: Supply, Extraction Processes and Use as Bio-Based Material, *Eur. Polym. J.*, 2019, **112**, 228–240, DOI: **10.1016/J.EURPOLYMJ.2019.01.007**.

4 N. Ghavidel and P. Fatehi, Interfacial and Emulsion Characteristics of Oil-Water Systems in the Presence of Polymeric Lignin Surfactant, *Langmuir*, 2021, **37**(11), 3346–3358, DOI: **10.1021/ACS.LANGMUIR.0C03458/SUPPL_FILE/LA0C03458_SI_001.PDF**.

5 B. V. K. J. Schmidt, V. Molinari, D. Esposito, K. Tauer and M. Antonietti, Lignin-Based Polymeric Surfactants for Emulsion Polymerization, *Polym.*, 2017, **112**, 418–426, DOI: **10.1016/J.POLYMER.2017.02.036**.

6 M. A. Jedrzejczyk, S. Van den Bosch, J. Van Aelst, K. Van Aelst, P. D. Kouris, M. Moalin, G. R. M. M. Haenen, M. D. Boot, E. J. M. Hensen, B. Lagrain, B. F. Sels and K. V. Bernaerts, Lignin-Based Additives for Improved Thermo-Oxidative Stability of Biolubricants, *ACS Sustain. Chem. Eng.*, 2021, **9**(37), 12548–12559, DOI: **10.1021/acssuschemeng.1c02799**.

7 S. Domenek, A. Louaifi, A. Guinault and S. Baumberger, Potential of Lignins as Antioxidant Additive in Active Biodegradable Packaging Materials, *J. Polym. Environ.*, 2013, **21**(3), 692–701, DOI: **10.1007/S10924-013-0570-6/METRICS**.

8 C. H. M. Camargos and C. A. Rezende, Antisolvent versus Ultrasonication: Bottom-up and Top-down Approaches to Produce Lignin Nanoparticles (LNPs) with Tailored Properties, *Int. J. Biol. Macromol.*, 2021, **193**, 647–660, DOI: **10.1016/J.IJBIOMAC.2021.10.094**.

9 M. Österberg, M. H. Sipponen, B. D. Mattos and O. J. Rojas, Spherical Lignin Particles: A Review on Their Sustainability and Applications, *Green Chem.*, 2020, **22**(9), 2712–2733, DOI: **10.1039/D0GC00096E**.

10 S. Gillet, M. Aguedo, L. Petitjean, A. R. C. Morais, A. M. Da Costa Lopes, R. M. Łukasik and P. T. Anastas, Lignin Transformations for High Value Applications: Towards Targeted Modifications Using Green Chemistry, *Green Chem.*, 2017, **19**(18), 4200–4233, DOI: **10.1039/C7GC01479A**.

11 S. Iravani and R. S. Varma, Greener Synthesis of Lignin Nanoparticles and Their Applications, *Green Chem.*, 2020, **22**(3), 612–636, DOI: **10.1039/C9GC02835H**.

12 M. Mariana, T. Alfatah, H. P. S. Abdul Khalil, E. B. Yahya, N. G. Olaiya, A. Nuryawan, E. M. Mistar, C. K. Abdullah, S. N. Abdulmadjid and H. Ismail, A Current Advancement on the Role of Lignin as Sustainable Reinforcement Material in Biopolymeric Blends, *J. Mater. Res. Technol.*, 2021, **15**, 2287–2316, DOI: **10.1016/J.JMRT.2021.08.139**.

13 A. Brandt, J. Gräsvik, J. P. Hallett and T. Welton, Deconstruction of Lignocellulosic Biomass with Ionic Liquids, *Green Chem.*, 2013, **15**(3), 550–583, DOI: **10.1039/C2GC36364J**.

14 X. Shi, X. Wang, B. Tang, Z. Dai, K. Chen and J. Zhou, Impact of Lignin Extraction Methods on Microstructure and

Mechanical Properties of Lignin-Based Carbon Fibers, *J. Appl. Polym. Sci.*, 2018, **135**(10), 45580, DOI: 10.1002/APP.45580.

15 J. H. Lora and W. G. Glasser, Recent Industrial Applications of Lignin: A Sustainable Alternative to Nonrenewable Materials, *J. Polym. Environ.*, 2002, **10**(1–2), 39–48, DOI: 10.1023/A:1021070006895/METRICS.

16 M. Lin, L. Yang, H. Zhang, Y. Xia, Y. He, W. Lan, J. Ren, F. Yue and F. Lu, Revealing the Structure-Activity Relationship between Lignin and Anti-UV Radiation, *Ind. Crops Prod.*, 2021, **174**, 114212, DOI: 10.1016/J.INDCROP.2021.114212.

17 P. Figueiredo, K. Lintinen, A. Kiriazis, V. Hynninen, Z. Liu, T. Bauleth-Ramos, A. Rahikkala, A. Correia, T. Kohout, B. Sarmento, J. Yli-Kauhaluoma, J. Hirvonen, O. Ikkala, M. A. Kostiainen and H. A. Santos, In Vitro Evaluation of Biodegradable Lignin-Based Nanoparticles for Drug Delivery and Enhanced Antiproliferation Effect in Cancer Cells, *Biomaterials*, 2017, **121**, 97–108, DOI: 10.1016/J.BIOMATERIALS.2016.12.034.

18 D. Piccinino, E. Capecchi, L. Botta, P. Bollella, R. Antiochia, M. Crucianelli and R. Saladino, Layer by Layer Supported Laccase on Lignin Nanoparticles Catalyzes the Selective Oxidation of Alcohols to Aldehydes, *Catal. Sci. Technol.*, 2019, **9**(15), 4125–4134, DOI: 10.1039/C9CY00962K.

19 A. G. Morena and T. Tzanov, Antibacterial Lignin-Based Nanoparticles and Their Use in Composite Materials, *Nanoscale Adv.*, 2022, **4**(21), 4447–4469, DOI: 10.1039/D2NA00423B.

20 A. G. Morena and T. Tzanov, Antibacterial Lignin-Based Nanoparticles and Their Use in Composite Materials, *Nanoscale Adv.*, 2022, **4**(21), 4447, DOI: 10.1039/D2NA00423B.

21 S. Iravani and R. S. Varma, Greener Synthesis of Lignin Nanoparticles and Their Applications, *Green Chem.*, 2020, **22**(3), 612–636, DOI: 10.1039/C9GC02835H.

22 E. Capecchi, E. Tomaino, D. Piccinino, P. E. Kidibule, M. Fernández-Lobato, D. Spinelli, R. Pogni, A. G. Cabado, J. Lago and R. Saladino, Nanoparticles of Lignins and Saccharides from Fishery Wastes as Sustainable UV-Shielding, Antioxidant, and Antimicrobial Biofillers, *Biomacromolecules*, 2022, **23**(8), 3154–3164, DOI: 10.1021/acs.biomac.2c00236.

23 D. Kai, M. J. Tan, P. L. Chee, Y. K. Chua, Y. L. Yap and X. J. Loh, Towards Lignin-Based Functional Materials in a Sustainable World, *Green Chem.*, 2016, **18**(5), 1175–1200, DOI: 10.1039/C5GC02616D.

24 W. D. H. Schneider, A. J. P. Dillon and M. Camassola, Lignin Nanoparticles Enter the Scene: A Promising Versatile Green Tool for Multiple Applications, *Biotechnol. Adv.*, 2021, **47**, 107685, DOI: 10.1016/J.BIOTECHADV.2020.107685.

25 W. Yang, E. Fortunati, D. Gao, G. M. Balestra, G. Giovanale, X. He, L. Torre, J. M. Kenny and D. Puglia, Valorization of Acid Isolated High Yield Lignin Nanoparticles as Innovative Antioxidant/Antimicrobial Organic Materials, *ACS Sustain. Chem. Eng.*, 2018, **6**(3), 3502–3514, DOI: 10.1021/acssuschemeng.7b03782.

26 E. Lizundia, I. Armentano, F. Luzi, F. Bertoglio, E. Restivo, L. Visai, L. Torre and D. Puglia, Synergic Effect of Nanolignin and Metal Oxide Nanoparticles into Poly(L-Lactide) Bionanocomposites: Material Properties, Antioxidant Activity, and Antibacterial Performance, *ACS Appl. Bio Mater.*, 2020, **2020**, 5263–5274, DOI: 10.1021/acsabm.0c00637.

27 Y. N. Slavin, K. Ivanova, J. Hoyo, I. Perelshtein, G. Owen, A. Haegert, Y.-Y. Lin, S. LeBihan, A. Gedanken, U. O. Häfeli, T. Tzanov and H. Bach, Novel Lignin-Capped Silver Nanoparticles against Multidrug-Resistant Bacteria, *ACS Appl. Mater. Interfaces*, 2021, **13**(19), 22098–22109, DOI: 10.1021/acsami.0c16921.

28 C. H. M. Camargos and C. A. Rezende, Antisolvent versus Ultrasonication: Bottom-up and Top-down Approaches to Produce Lignin Nanoparticles (LNPs) with Tailored Properties, *Int. J. Biol. Macromol.*, 2021, **193**, 647–660, DOI: 10.1016/j.ijbiomac.2021.10.094.

29 V. Noronha, C. Camargos, J. Jackson, A. Souza Filho, A. Paula, C. Rezende and A. Faria, Physical Membrane-Stress-Mediated Antimicrobial Properties of Cellulose Nanocrystals, *ACS Sustain. Chem. Eng.*, 2021, **9**(8), 3203–3212, DOI: 10.1021/acssuschemeng.0c08317.

30 V. T. Noronha, J. C. Jackson, C. H. M. Camargos, A. J. Paula, C. A. Rezende and A. F. Faria, Attacking–Attacking Anti-Biofouling Strategy Enabled by Cellulose Nanocrystals–Silver Materials, *ACS Appl. Bio Mater.*, 2022, **5**(3), 1025–1037, DOI: 10.1021/acsabm.1c00929.

31 A. Faria, F. Perreault and M. Elimelech, Elucidating the Role of Oxidative Debris in the Antimicrobial Properties of Graphene Oxide, *ACS Appl. Nano Mater.*, 2018, **1**(3), 1164–1174, DOI: 10.1021/acsanm.7b00332.

32 F. Perreault, A. F. de Faria, S. Nejati and M. Elimelech, Antimicrobial Properties of Graphene Oxide Nanosheets: Why Size Matters, *ACS Nano*, 2015, **9**(7), 7226–7236, DOI: 10.1021/acsnano.5b02067.

33 S. Romero-Vargas Castrillón, F. Perreault, A. Fonseca de Faria and M. Elimelech, Interaction of Graphene Oxide with Bacterial Cell Membranes: Insights from Force Spectroscopy, *Environ. Sci. Technol. Lett.*, 2015, **2**(4), 112–117, DOI: 10.1021/acs.estlett.5b00066.

34 O. Carmel-Harel and G. Storz, Roles of the Glutathione- and Thioredoxin-Dependent Reduction Systems in the Escherichia Coli and Saccharomyces Cerevisiae Responses to Oxidative Stress, *Annu. Rev. Microbiol.*, 2000, **54**(1), 439–461, DOI: 10.1146/annurev.micro.54.1.439.

35 R. C. Fahey, W. C. Brown, W. B. Adams and M. B. Worsham, Occurrence of Glutathione in Bacteria, *J. Bacteriol.*, 1978, **133**(3), 1126, DOI: 10.1007/s10541-005-0248-3.

36 K. A. Mahmoud, J. A. Mena, K. B. Male, S. Hrapovic, A. Kamen and J. H. T. Luong, Effect of Surface Charge on the Cellular Uptake and Cytotoxicity of Fluorescent Labeled Cellulose Nanocrystals, *ACS Appl. Mater. Interfaces*, 2010, **2**(10), 2924–2932, DOI: 10.1021/am1006222.

37 S. Iravani and R. S. Varma, Greener Synthesis of Lignin Nanoparticles and Their Applications, *Green Chem.*, 2020, **7**, 612–636, DOI: 10.1039/c9gc02835h.

38 W. Yang, E. Fortunati, D. Gao, G. M. Balestra, G. Giovanale, X. He, L. Torre, J. J. Kenny and D. Puglia, Valorization of acid isolated high yield lignin nanoparticles as innovative antioxidant/antimicrobial organic materials, *ACS Sustainable Chem. Eng.*, 2018, **6**(3), 3502–3514, DOI: **10.1021/acssuschemeng.7b03782**.

39 E. Gerbin, G. N. Rivière, L. Foulon, Y. M. Frapart, B. Cottyn, M. Pernes, C. Marcuello, B. Godon, A. Gainvors-Claisse, D. Crônier, A. Majira, M. Österberg, B. Kurek, S. Baumberger and V. Aguié-Béghin, Tuning the functional properties of lignocellulosic films by controlling the molecular and supramolecular structure of lignin, *Int. J. Biol. Macromol.*, 2021, **181**, 136–149, DOI: **10.1016/j.ijbiomac.2021.03.081**.

40 S. Gurunathan, J. W. Han, A. Abdal Dayem, V. Eppakayala and J. H. Kim, Oxidative Stress-Mediated Antibacterial Activity of Graphene Oxide and Reduced Graphene Oxide in Pseudomonas Aeruginosa, *Int. J. Nanomed.*, 2012, **7**, 5901–5914, DOI: **10.2147/IJN.S37397**.

41 I. Sengupta, P. Bhattacharya, M. Talukdar, S. Neogi, S. K. Pal and S. Chakraborty, Bactericidal Effect of Graphene Oxide and Reduced Graphene Oxide: Influence of Shape of Bacteria, *Colloids Interface Sci. Commun.*, 2019, **28**, 60–68, DOI: **10.1016/j.colcom.2018.12.001**.

42 N. Maldonado-Carmona, G. Marchand, N. Villandier, T. S. Ouk, M. M. Pereira, M. J. F. Calvete, C. A. Calliste, A. Żak, M. Piksa, K. J. Pawlik, K. Matczyszyn and S. Leroy-Lhez, Porphyrin-Loaded Lignin Nanoparticles Against Bacteria: A Photodynamic Antimicrobial Chemotherapy Application, *Front. Microbiol.*, 2020, **11**, 606185, DOI: **10.3389/FMICB.2020.606185**.

43 W. Yang, E. Fortunati, D. Gao, G. M. Balestra, G. Giovanale, X. He, L. Torre, J. M. Kenny and D. Puglia, Valorization of Acid Isolated High Yield Lignin Nanoparticles as Innovative Antioxidant/Antimicrobial Organic Materials, *ACS Sustain. Chem. Eng.*, 2018, **6**(3), 3502–3514, DOI: **10.1021/acssuschemeng.7b03782**.

44 S. Paul, N. S. Thakur, S. Chandna, Y. N. Reddy and J. Bhaumik, Development of a Light Activatable Lignin Nanosphere Based Spray Coating for Bioimaging and Antimicrobial Photodynamic Therapy, *J. Mater. Chem. B*, 2021, **9**(6), 1592–1603, DOI: **10.1039/D0TB02643C**.

45 A. G. Morena, A. Bassegoda, M. Natan, G. Jacobi, E. Banin and T. Tzanov, Antibacterial Properties and Mechanisms of Action of Sonoenzymatically Synthesized Lignin-Based Nanoparticles, *ACS Appl. Mater. Interfaces*, 2022, **14**(33), 37270–37279, DOI: **10.1021/acsami.2c05443**.

46 X. Dong, M. Dong, Y. Lu, A. Turley, T. Jin and C. Wu, Antimicrobial and Antioxidant Activities of Lignin from Residue of Corn Stover to Ethanol Production, *Ind. Crops Prod.*, 2011, **34**(3), 1629–1634, DOI: **10.1016/j.indcrop.2011.06.002**.

47 L. Bouarab-Chibane, V. Forquet, P. Lantéri, Y. Clément, L. Léonard-Akkari, N. Oulahal, P. Degraeve and C. Bordes, Antibacterial Properties of Polyphenols: Characterization and QSAR (Quantitative Structure–Activity Relationship) Models, *Front. Microbiol.*, 2019, **10**(APR), 440698, DOI: **10.3389/fmicb.2019.00829**.

48 X. Dong, M. Dong, Y. Lu, A. Turley, T. Jin and C. Wu, Antimicrobial and Antioxidant Activities of Lignin from Residue of Corn Stover to Ethanol Production, *Ind. Crops Prod.*, 2011, **34**(3), 1629–1634, DOI: **10.1016/j.indcrop.2011.06.002**.

49 L. Bouarab-Chibane, V. Forquet, P. Lantéri, Y. Clément, L. Léonard-Akkari, N. Oulahal, P. Degraeve and C. Bordes, Antibacterial Properties of Polyphenols: Characterization and QSAR (Quantitative Structure–Activity Relationship) Models, *Front. Microbiol.*, 2019, **10**(APR), 440698, DOI: **10.3389/fmicb.2019.00829**.

50 E. Lizundia, I. Armentano, F. Luzi, F. Bertoglio, E. Restivo, L. Visai, L. Torre and D. Puglia, Synergic Effect of Nanolignin and Metal Oxide Nanoparticles into Poly(l-Lactide) Bionanocomposites: Material Properties, Antioxidant Activity, and Antibacterial Performance, *ACS Appl. Bio Mater.*, 2020, **3**(8), 5263–5274, DOI: **10.1021/ACSABM.0C00637**.

51 S. S. Nanda, S. S. A. An and D. K. Yi, Oxidative Stress and Antibacterial Properties of a Graphene Oxide-Cystamine Nanohybrid, *Int. J. Nanomed.*, 2015, **10**, 549–556, DOI: **10.2147/IJN.S75768**.

52 C. D. Vecitis, K. R. Zodrow, S. Kang and M. Elimelech, Electronic-Structure-Dependent Bacterial Cytotoxicity of Single-Walled Carbon Nanotubes, *ACS Nano*, 2010, **4**(9), 5471–5479, DOI: **10.1021/nn101558x**.

53 L. R. Arias and L. Yang, Inactivation of Bacterial Pathogens by Carbon Nanotubes in Suspensions, *Langmuir*, 2009, **25**(5), 3003–3012, DOI: **10.1021/la802769m**.

54 A. Borges, C. Ferreira, M. J. Saavedra and M. Simões, Antibacterial Activity and Mode of Action of Ferulic and Gallic Acids against Pathogenic Bacteria, *Microb. Drug Resist.*, 2013, **19**(4), 256–265, DOI: **10.1089/mdr.2012.0244**.

55 L. Qin, W. C. Li, L. Liu, J. Q. Zhu, X. Li, B. Z. Li and Y. J. Yuan, Inhibition of Lignin-Derived Phenolic Compounds to Cellulase, *Biotechnol. Biofuels*, 2016, **9**(1), 70, DOI: **10.1186/s13068-016-0485-2**.

56 A. Renzetti, J. W. Betts, K. Fukumoto and R. N. Rutherford, Antibacterial Green Tea Catechins from a Molecular Perspective: Mechanisms of Action and Structure-Activity Relationships, *Food Funct.*, 2020, **1**, 9370–9396, DOI: **10.1039/d0fo02054k**.

57 A. O. Gill and R. A. Holley, Mechanisms of Bactericidal Action of Cinnamaldehyde against Listeria Monocytogenes and of Eugenol against L. Monocytogenes and Lactobacillus Sakei, *Appl. Environ. Microbiol.*, 2004, **70**(10), 5750–5755, DOI: **10.1128/AEM.70.10.5750-5755.2004**.

58 F. M. C. Freitas, M. A. Cerqueira, C. Gonçalves, S. Azinheiro, A. Garrido-Maestu, A. A. Vicente, L. M. Pastrana, J. A. Teixeira and M. Michelin, Green Synthesis of Lignin Nano- and Micro-Particles: Physicochemical Characterization, Bioactive Properties and Cytotoxicity Assessment, *Int. J. Biol. Macromol.*, 2020, **163**, 1798–1809, DOI: **10.1016/j.ijbiomac.2020.09.110**.

59 X. Dong, M. Dong, Y. Lu, A. Turley, T. Jin and C. Wu, Antimicrobial and Antioxidant Activities of Lignin from Residue of Corn Stover to Ethanol Production, *Ind. Crops Prod.*, 2011, **34**(3), 1629–1634, DOI: **10.1016/j.indcrop.2011.06.002**.

60 T. Dizhbite, G. Telysheva, V. Jurkjane and U. Viesturs, Characterization of the Radical Scavenging Activity of Lignins - Natural Antioxidants, *Bioresour. Technol.*, 2004, **95**(3), 309–317, DOI: **10.1016/j.biortech.2004.02.024**.

61 R. Castaneda-Arriaga, A. Pérez-González, M. Reina, J. R. Alvarez-Idaboy and A. Galano, Comprehensive Investigation of the Antioxidant and Pro-Oxidant Effects of Phenolic Compounds: A Double-Edged Sword in the Context of Oxidative Stress?, *J. Phys. Chem. B*, 2018, **122**(23), 6198–6214, DOI: **10.1021/acs.jpcb.8b03500**.

62 M. Khatun, Z. Khatun, M. R. Karim, M. R. Habib, M. H. Rahman and M. A. Aziz, Green Synthesis of Silver Nanoparticles Using Extracts of Mikania Cordata Leaves and Evaluation of Their Antioxidant, Antimicrobial and Cytotoxic Properties, *Food Chem. Adv.*, 2023, **3**, 100386, DOI: **10.1016/J.FOCHA.2023.100386**.

63 A. G. Morena and T. Tzanov, Antibacterial Lignin-Based Nanoparticles and Their Use in Composite Materials, *Nanoscale Adv.*, 2022, **11**, 4447–4469, DOI: **10.1039/d2na00423b**.

64 B. Ndaba, A. Roopnarain, M. O. Daramola and R. Adeleke, Influence of Extraction Methods on Antimicrobial Activities of Lignin-Based Materials: A Review, *Sustainable Chem. Pharm.*, 2020, **1**, 100342, DOI: **10.1016/j.scp.2020.100342**.

65 M. Chen, Y. Li, H. Liu, D. Zhang, Q. S. Shi, X. Q. Zhong, Y. Guo and X. B. Xie, High Value Valorization of Lignin as Environmental Benign Antimicrobial, *Mater. Today Bio*, 2023, **18**, 100520, DOI: **10.1016/j.mtbio.2022.100520**.

66 F. M. C. Freitas, M. A. Cerqueira, C. Gonçalves, S. Azinheiro, A. Garrido-Maestu, A. A. Vicente, L. M. Pastrana, J. A. Teixeira and M. Michelin, Green Synthesis of Lignin Nano- and Micro-Particles: Physicochemical Characterization, Bioactive Properties and Cytotoxicity Assessment, *Int. J. Biol. Macromol.*, 2020, **163**, 1798–1809, DOI: **10.1016/j.ijbiomac.2020.09.110**.